Article:

Sofotasiou, P., Calautit, J.K., Hughes, B.R. et al. (1 more author) (2016) Towards an integrated computational method to determine internal spaces for optimum environmental conditions. Computers & Fluids, 127. pp. 146-160. ISSN 0045-7930

https://doi.org/10.1016/j.compfluid.2015.12.015

Towards an integrated computational method to determine internal spaces for optimum environmental conditions

Polytimi Sofotasiou[a*], John Kaiser Calautit[a], Ben Richard Hughes[a], Dominic O'Connor[a]

[a] School of Mechanical Engineering, University of Sheffield, Sheffield S10 2TN, UK

[*]Corresponding author. tel: +44(0) 7479232058, e-mail: psofotasiou1@sheffield.ac.uk

Abstract

Computational Fluid Dynamics tools and Response Surface Methodology optimization techniques were coupled for the evaluation of an optimum window opening design that improves the ventilation efficiency in a naturally-ventilated building. The multi-variable optimization problem was based on Design of Experiments analysis and the Central Composite Design method for the sampling process and estimation of quadratic models for the response variables. The Screening optimization method was used for the generation of the optimal design solution. The generated results indicated a good performance of the estimated response surface revealing the strength correlations between the parameters. Window width was found to have greater impact on the flow rate values with correlation coefficient of 73.62%, in comparison to the standard deviation 55.68%, where the window height prevails with correlation coefficient of 96.94% and 12.35% for the flow rate. The CFD results were validated against wind tunnel experiments and the optimization solution was verified with simulation runs, proving the accuracy of the methodology followed, which is applicable to numerous environmental design problems.

Keywords: Computational fluid dynamics (CFD); Response Surface Methodology (RSM); Optimization; Natural ventilation

1. Introduction

A successful building design improves the quality of life and facilitates the functional needs of the users. However, the achievement of acceptable design solutions presupposes the contribution of rational multidisciplinary decisions [1]. An important and mandatory step prior to every engineering solution is the conceptual design phase that tends to establish the holistic integrity of the design. The development of software tools has facilitated the decision-making process, by offering the opportunity to evaluate the performance and efficiency of the initial design concept under numerous objective parameters during the conceptual design phase.

Computational Fluid Dynamics (CFD) software is used to perform multiple types of analysis, regarding a rational approach to design investigation that enables the simulation of air flow and prediction of physical phenomena within building spaces [2]. This technique has been adopted by numerous researchers, to study the thermal comfort of occupants in buildings [3], the positioning of building services [4], natural ventilation [5], heat transfer effects [6], contaminant dispersion [7] and the interaction between indoor and outdoor environments [8].

This study presents an integrated computational method to optimise design spaces in the built environment. The work is based on simulation-driven optimisation techniques, using a CFD simulation software integrated with Response Surface Methodology-based design optimisation algorithms and validated against wind tunnel experiments. The method is applied to a generic cross-ventilated building structure to investigate natural ventilation efficiency. Since 1992 [9] up to present [10], studies on cross-ventilated buildings have been performed using CFD techniques and validated with real scale measurements, wind tunnel experiments and flow visualization methods [11]. However, the increasing need for adopting integrated design solutions demands further information beyond what it is offered by the investigation of the naturally occurring wind flow in buildings, and it is this research gap under investigation here.

2. Previous related work

Stavrakakis et al. (2012) investigated the optimum window-opening configuration, to improve the indoor thermal comfort in a naturally-ventilated building (NVB). Using a coupled CFD-ANN (Artificial Neutral Network) technique that enabled the evaluation of 126 data pairs to minimise discomfort for 3 different activity levels. On the investigation of the influential behaviour of the air speed and direction towards the ventilation rates in NVB, Shen et al., (2012) combined CFD and Response Surface Methodology (RSM) optimization techniques. They evaluated different Design of Experiment (DoE) methods for the generation of experimental models in a stand-alone software. The obtained results were validated with CFD simulation cases.

In a more recent study, Shen et al., (2013) assessed the performance of different DoE methods on the estimation of the ventilation rate in a naturally ventilated livestock. The parameters evaluated were the window opening characteristics and wind conditions. The results indicated that the most accurate response surface model was developed by the Box-Behnken design, followed by the central composite rotation design (CCRD) method. The work also highlighted that the performance of the DoE method may differ, depending on the case study. On the optimization of ventilation efficiency and indoor homogeneous conditions in livestock buildings, Norton et al. (2010) employed CFD tools and Box-Bohnken design methods for the generation of a response function based on the geometrical characteristics of the building. The verified RSM method indicated that the environmental heterogeneity is more correlated to the geometrical characteristics of the building and particularly when the most restrictive eave opening conditions, regarding porosity and height, are applied.

Both ANN and RSM are well-recognised techniques that enable the approximation of the interrelated nature of the independent design parameters and their design solutions [15]. However, the aforementioned research topics within the NVB framework, generated the experimental case studies in independent software and used CFD codes to perform parametric analyses and/ or validation of the results.

In this study, a commercial CFD software integrated with RSM optimisation techniques is employed to present a parametric simulation method for the analysis and optimisation of a simple cross-ventilated building. The RSM technique is used to determine the interrelationships between the design parameters and design responses. The Screening optimization technique is employed to identify the optimum window opening dimensions that improve the natural ventilation efficiency in terms of the air flow rate and flow homogeneity. The CFD results were validated against wind tunnel experiments to establish the accuracy of the method.

In Section 3, the theoretical background of the RSM, which is used in the parametric-optimization study, is briefly presented. In Section 4, the case study is introduced followed by the CFD methodology, results and validation study. The optimisation methodology is presented in Section 5, along with the interpretation and verification of results. Finally, the discussion and conclusions are covered in Section 6 and 7 respectively.

3. Response Surface Methodology (RSM)

Pioneers in the exploration of the impact of the design parameters on several design responses were Hotelling (1941) and Friedman and Savage (1947). In mathematical terms, the unknown functional relationship between the design parameters (x) and their design responses (y) can be described by the low-degree polynomial model given by the Eq. (1):

$$y = f(x, \theta) + \varepsilon \qquad \text{Eq. (1)}$$

where ε is treated as a statistical error. By employing mathematical and statistical methods, first-order (Eq. (2)) and second-order (Eq. (3)) polynomial regression models are constructed, based on physical or computer experiments [18].

$$\eta = \beta_0 + \beta_1 x_1 + \cdots + \beta_k x_k \qquad \text{Eq. (2)}$$

$$\eta = \beta_0 + \sum_{i=1}^{k} \beta_i x_i + \sum_{i=1}^{k} \beta_{ii} x_i^2 + \sum_{\substack{i=1 \\ i<j}}^{k} \sum_{j=1}^{k} \beta_{ij} x_i x_j \qquad \text{Eq. (3)}$$

where η represents a design solution (i.e. velocity, temperature, stresses, etc), x_1, x_2, …, x_k the design variables (i.e. height, thickness, load, etc) and β_0, β_1,…, β_k the unknown regression coefficients.

Box and Wilson (1951) introduced a statistical tool that enables the evaluation of several design parameters, targeting an improved design solution (or response) by satisfying specific requirements. They defined the “experimental region” as the region within which the design parameters vary and the optimum design solution is localized, with the minimum possible number of conducted experiments. This method is known as Response Surface Methodology (RSM) and targets finding an improved, if not optimum, response of given controllable variables.

The RSM calculates approximate values for the regression coefficients, based on the evaluation of either experimental or simulation results generated for a specific number of sample design points. Once the best fitted approximation function is found, several design combinations can be examined, without the need to conduct deterministic response analysis that is an extremely time-consuming process. It is therefore apparent that the performance of a fully accurate design study may necessitate the simultaneous consideration of several independent design variables, resulting in complex mathematical functions/systems.

RSM has been widely used in various projects and disciplines, due to its advantageous performance in approaching mathematically the behaviour of multiscale phenomena, regardless of the nature of the studied parameters [16]. The integration of this method with expensive computer simulation codes has launched a new generation of research studies, which allows the optimization of designs with either large or small number of input and output parameters.

Fegade and Patel (2013) studied a parametric finite element model of a rotor, by employing Design of Experiments (DOE) techniques integrated in ANSYS simulation software. They performed 48 simulation runs, aiming at investigating the effect of different rotor diameters on the rotor's frequency. For the purpose of this, two levels factorial design with eleven input parameters per Plankett-Burman[1] design was considered and it two rotor diameters were found to have major impact on frequency for the fluid film.

Mandloi and Verma (2009) employed Central Composite Design (CCD) experimental design in order to improve the performance and efficiency of an in-cylinder engine intake port. Based on RSM from ANSYS software, they established a goal-driven optimum design solution, determined by independent geometrical characteristics.

Ng et al. (2008) evaluated the performance index of an air diffusion system integrated in a displacement-ventilated office. With the aid of commercial statistical and CFD software, they used RSM to predict the optimum position for the diffusers, the supply temperature and the exhaust position, in order to provide optimum thermal comfort in the space. The results obtained from the Box-Behnken design models were found to agree 95% with the CFD simulation results, indicating the accuracy of the method, as well as the very promising benefits and results.

4. Case study description

The achievement of an accurate and reliable simulation research study requires full compliance with the fundamental steps and in depth understanding of the CFD simulation and optimization processes. For the purpose of this, a simple benchmark building model was designed, as illustrated in Figure 1. The geometrical characteristics are based on a previously published research paper of Karava et al. (2011). The scaled building dimensions are 0.1m x 0.1m x 0.08m (L x W x H), wall depth of 0.002

[1] Plankett-Burman experimental design is a factional factorial design, which is manly used for the identification of the most important variables of a partly known system with a large number of independent factors [21].

m, and two window openings of 0.018m x 0.046m (H x W), placed on the opposite sides at the centres of the walls to promote natural airflow with the least resistance.

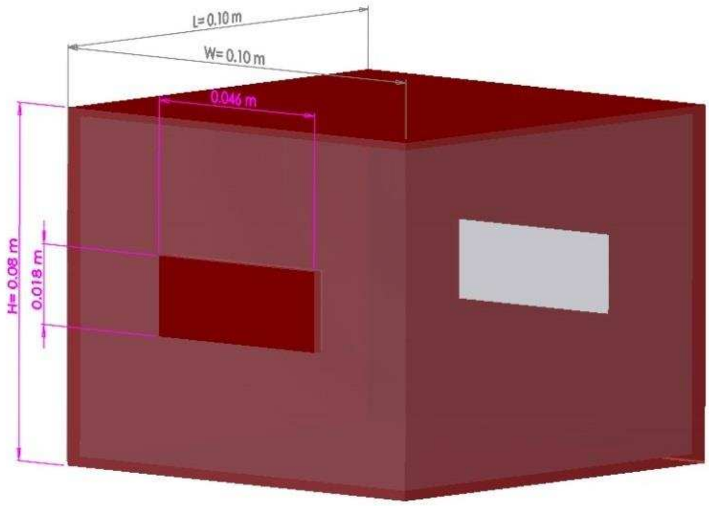

Figure 1 Dimensional characteristics of the case study building model.

4.1 CFD set-up

The CFD simulation analysis was performed with the commercial software ANSYS Workbench 15, since it comprises a complete interface for the implementation of the work. The study was conducted in three phases. The pre-processing phase included the creation of the building model and the domain geometry, and the generation of the computational mesh. The second phase comprised the solver, along with the selection of the transport equations, the physical models and the solver settings. Finally, in the post-processing phase, plots and graphs of the solutions were created and the results were interpreted.

4.2 Governing equations

The simulation of the natural ventilation phenomena was treated as steady and incompressible turbulent flow. The standard k-ε turbulence model was used with standard wall functions, since it is widely used in natural ventilation studies in buildings [11], [25], [26], [27], [28], [30]and it shows good performance when compared with wind tunnel experiments [29], [31], [32], [32][33]. Moreover, when empty rooms are studied, the standard k-ε and the RNG k-ε model have been proven to behave similarly [34], [35]. The governing equations of continuity (4), momentum (5), as well as the transport equations of the standard k-ε turbulence model (6 & 7) are presented below:

$$\frac{\partial \overline{u_i}}{\partial x_i} = 0 \qquad \text{Eq. (4)}$$

$$\frac{\partial \overline{u_i u_j}}{\partial x_j} = -\frac{1}{\rho}\frac{\partial \bar{p}}{\partial x_i} + \frac{\partial}{\partial x_j}\left(\upsilon\left(\frac{\partial \overline{u_i}}{\partial x_j} + \frac{\partial \overline{u_i}}{\partial x_i}\right)\right) \qquad \text{Eq. (5)}$$

$$\rho\frac{\partial k}{\partial t} + \rho u_i \frac{\partial k}{\partial x_i} = \frac{\partial}{\partial x_j}\left[\left(\frac{\mu+\mu_t}{\sigma_k}\right)\frac{\partial k}{\partial x_j}\right] + P - \rho\varepsilon \qquad \text{Eq. (6)}$$

$$\rho\frac{\partial \varepsilon}{\partial t} + \rho u_i \frac{\partial \varepsilon}{\partial x_i} = \frac{\partial}{\partial x_j}\left[\left(\frac{\mu+\mu_t}{\sigma_\varepsilon}\right)\frac{\partial \varepsilon}{\partial x_j}\right] + c_{\varepsilon 1}\frac{\varepsilon}{k}P - c_{\varepsilon 2}\frac{\rho\varepsilon^2}{k} \qquad \text{Eq. (7)}$$

where μ_t is the turbulent viscosity calculated by the equation $\mu_t = C_\mu \frac{k^2}{\varepsilon}$, with $C\mu=0.09$, $\bar{u}$ and $\bar{p}$ are the mean (time-averaged) components of velocity and pressure, $P = \frac{\mu_t}{\rho} S^2$ represents the production of turbulence, $S = \sqrt{2S_{ij}S_{ij}}$ the shear stress magnitude and $C\varepsilon_1=1.44$, $C\varepsilon_2=1.92$, $\sigma_k= 1.0$ and $\sigma_\varepsilon=1.3$ [37].

4.3 Computational geometry and mesh generation

The size of the computational domain was set according to the wind tunnel's working section dimensions that would be used in sequence for a scaled validation study [39]. More specifically, the domain had dimensions of 0.5m x 1.0m x 0.5m (W x L x H) (Figure 2), allowing a blockage ratio ($Area_{model}$ /$Area_{tunnel}$ x 100%) of 2.8%, which lies within the recommended values for accurate simulation studies of air flow around buildings located in open flat terrains [40].

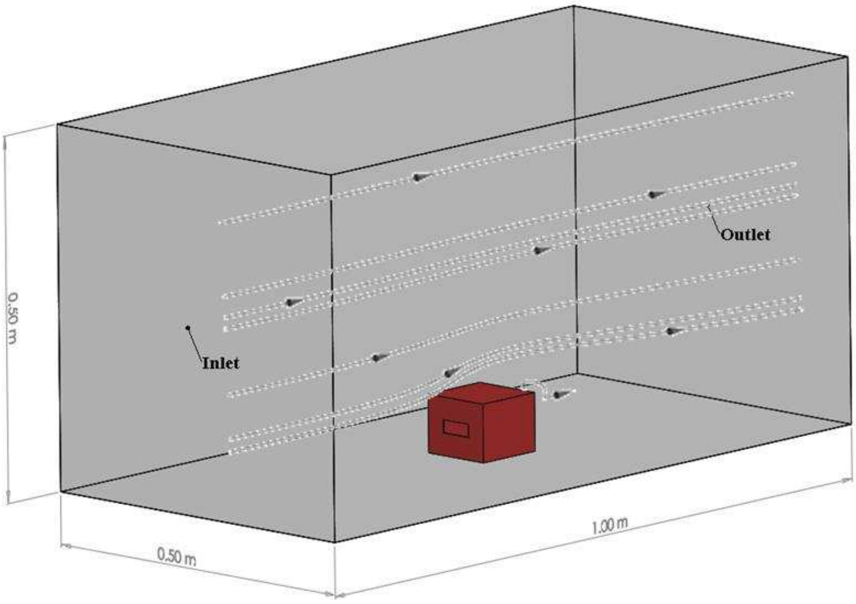

Figure 2 Computational domain and model positioning.

The simplicity of the geometry allowed the creation of a fully hexahedral mesh that enables better convergence behaviour. A finer grid was generated around the critical areas of the model, including the building edges, the window openings, as well as, the front, back and lateral flow paths around the building block. The rest of the domain was developed with high-resolution on the connections along the critical areas, starting with height of the neighbour cell at 0.002 m and an increasing size thereafter till the edges of the domain with a ratio of 1.2, leading to a coarser grid size, as illustrated in Figure 3.

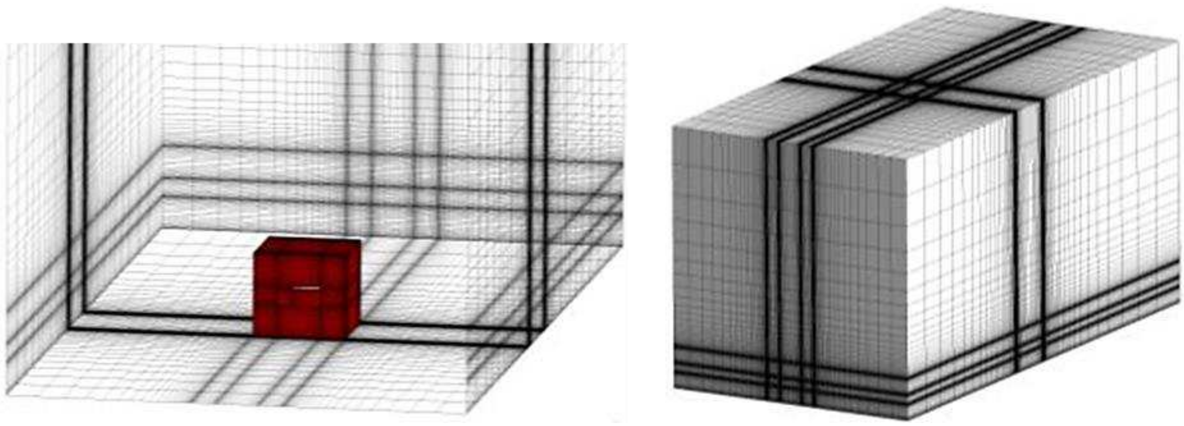

Figure 3 Computational surface grid of the simulation model (left) and the flow domain (right).

4.4 Grid Verification

In order to ensure grid independency, the volume adaptation method was used that enables the refinement and coarsening of the entire fluid volume. The initial mesh that was produced in ANSYS

Mesher, comprised of 1,071,790 hexahedral cells. The refinement and coarsening of the computational domain enabled the comparison of the average rates of air velocity in the two window openings. In the initial grid size of 1,071,790 cells, the average wind velocity value was equal to 1.88 m/s. The coarsening of the domain led to 647,542 hexahedral cells, with a magnitude of average wind velocity equal to 1.79 m/s. After the refinement of the computational domain, 1,236,636 hexahedral cells were produced, with an average wind speed equal to 1.92 m/s. The deviation of the average velocity magnitude from the medium grid was 4.8% for the coarse grid and 2.1% for the fine grid, as shown in Table 1. Thus, the medium size grid was selected for the simulation analysis, ensuring good performance, with reduced computational cost and without compromising the accuracy of the solution.

Table 1. Estimated error of average velocity magnitude at the two openings of the building block

Computational Grid Size	**Average Velocity (m/s)**	$\boldsymbol{\epsilon = (f_2 - f_1)/f_1}$ **100%**
Coarse: 647,542	1.79	4.8 %
Middle: 1,071,790	1.88	-
Fine: 1,236,636	1.92	2.1 %

4.5 Boundary conditions and solution settings

The boundary conditions set were similar to the one used in the research of Calautit and Hughes (2014), since the same wind tunnel facility was used. A constant wind profile was set at the inlet and zero static pressure at the outlet. At the side, top and ground walls of the domain, no-slip shear condition was applied with roughness height, k_s=0.001 m and roughness constant, C_s=0.5. The walls of the building block were set with similar roughness height of 0.001 m. The boundary conditions along with the solver settings are summarised in Table 2:

Table 2. Boundary conditions and solver settings for the simulation model

Inlet	Constant velocity U = 3m/s
Outlet	Zero pressure
Side, Top and Ground walls	k_s =0.001 m and Cs=0.5
Building walls	k_s=0.001 m and C_s=0.5
Turbulence model	Standard k-ε turbulence model
Scheme	SIMPLE
Spatial Discretization	Pressure: Standard, Momentum, Turbulence Kinetic Energy and Diss.Rate: Second Order

4.6 CFD results

The initial numerical simulation study generated results of the wind and pressure distributions inside and outside the building block. Figure 4 illustrates the dimensionless velocity patterns and the normalised vectors at the vertical cross section of the domain. The uniform velocity of 3 m/s (used also as reference velocity, U_{ref}) at the inlet resulted to a maximum velocity speed of 3.93 m/s and 2.88 m/s at the exterior and interior areas of the building respectively. According to the results, recirculation zones are developed below the openings of the upwind and downwind walls, as well as across the roof due to flow separation at the top front edge of the building block. At the interior, the air is driven directly from the one side to the other, due to the pressure difference between the two opposite window openings. Recirculation zones are created at both top and bottom parts of the interior windward wall.

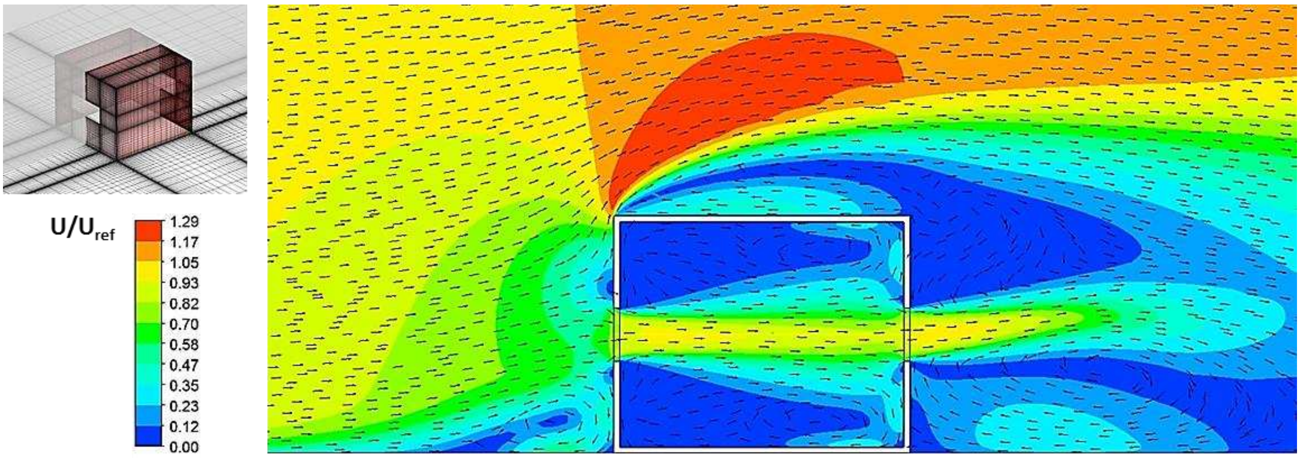

Figure 4 Dimensionless velocity contours and normalised vectors on the vertical plane in the middle of the building block; as U_{ref} was taken the inlet velocity magnitude of 3m/s.

In case of naturally ventilated buildings, the attainment of sufficient ventilation is important for the provision of comfortable indoor environments, mainly counted in terms of air volume induced in the occupied spaces and in terms of homogeneity, for equal flow distribution. Thus, the evaluation of the results was focused on two parameters. The first one was the volumetric flow rate (Q), as an indicator of the air volume passing through the windward window per unit time and the second one was the standard deviation of velocities at the building interior, to assess the homogeneity of the flow. These parameters can be calculated by the Eq. (8) and (9) below:

$$Q = \frac{\dot{m}}{\rho} \qquad \text{Eq. (8)}$$

$$SD = \sqrt{\frac{\sum(U_i - \bar{U})^2}{n}} \qquad \text{Eq. (9)}$$

where Q is the flow rate (m^3/s), $\dot{m}$ is the mass flow rate (kg/s), ρ is the air density (1.2 kg/m^3), SD is the standard deviation of velocities, U_i is the velocity at interior location i (m/s), $\bar{U}$ is the mean velocity at the interior of the block (m/s) and n is the number of computational cells at the interior of the block. The expressions were generated in ANSYS post processing and the graphical illustrations along with the obtained numerical values are presented in Table 3.

Table 3. Graphical illustration of the CFD simulation results

Expression	**Value**	**Graphic Illustration**
Flow Rate Q (m^3/s)	1.81×10^{-3}	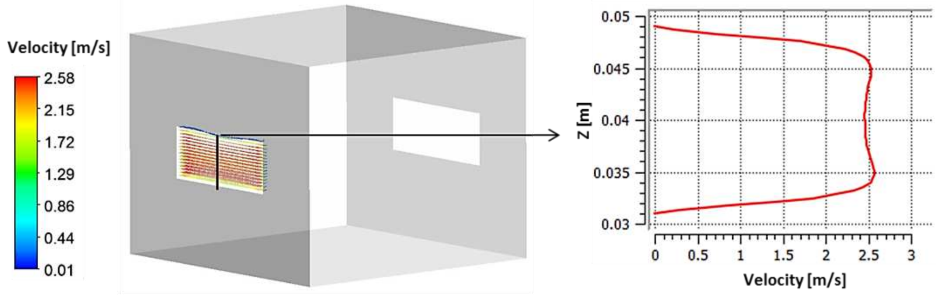 Velocity vectors at the windward window opening (left) and vertical velocity distribution in the middle of the opening (right)
St_Dev_Vel (m/s)	0.512	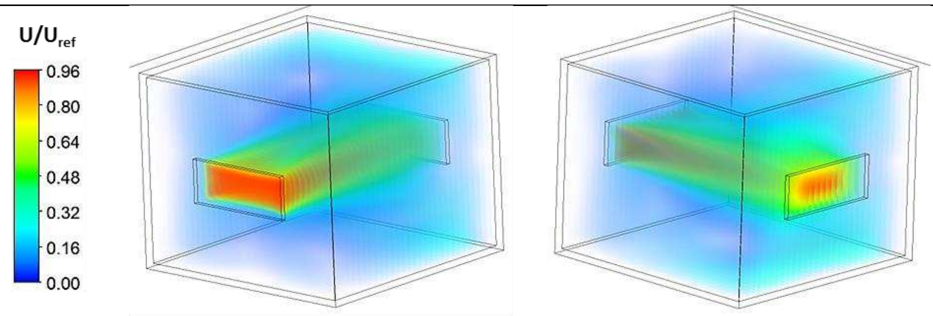 Dimensionless velocity magnitudes at the interior of the building block, on the windward (left) and leeward side (right)

It was observed that the incoming air stream through the front window opening developed an almost symmetrical distribution of velocity magnitudes, with a maximum value of 2.58 m/. In the interior of the building block, the highest velocity magnitudes were recorded at the horizontal flow path between the two openings. The percentage distribution of velocity magnitudes are presented in Figure 5, indicating that around 48% of the internal points have velocity magnitudes lower than 0.29 m/s. On the windward wall of the building model, recirculation zones were developed on top and below the window opening, creating intensively ventilated areas, compared to the leeward side of the building, where calm zones were observed, making the internal airflow relatively heterogeneous.

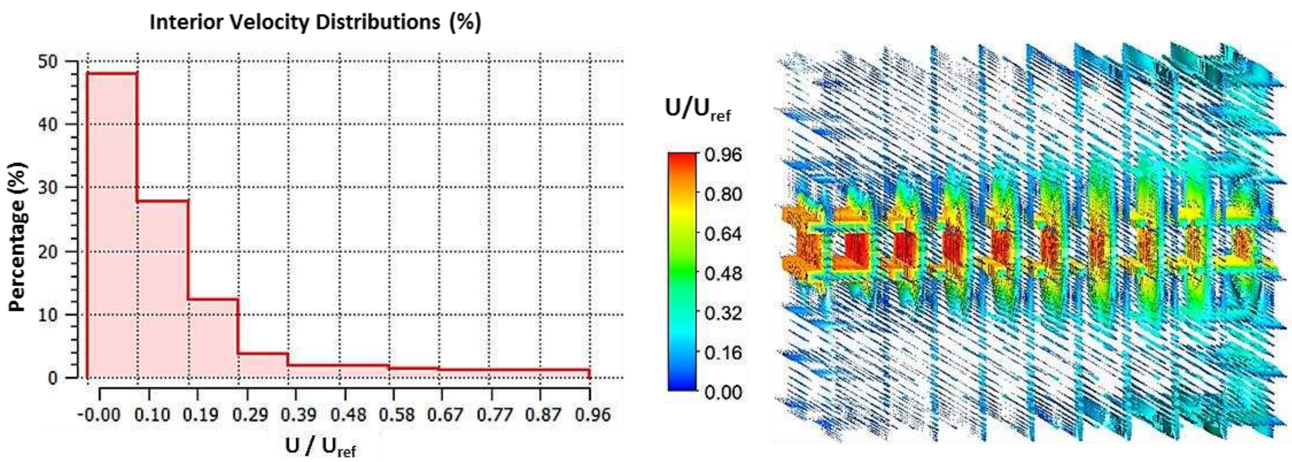

Figure 5 Histogram of dimensionless velocity distribution (left) and dimensionless velocity vectors (right) at the interior of the building block.

4.7 CFD validation

4.7.1 Inlet velocity profile

For the current study a constant velocity profile was set as inlet boundary condition, in order to match the one produced from the available wind tunnel facility, in the knowledge that it cannot represent a realistic flow field. The generated velocity profile at the longitudinal direction in the centre of the building block is illustrated in Figure 6, by the red line. The results are compared with the one produced by the study of Ramponi and Blocken (2012) (see Figure 6 black dashed line), in which a logarithmic velocity profile was applied at the inlet.

According to Chen and Srebric (2002) studies with significant level of accuracy are produced, provided that the generated trends are consistent. It is also highlighted the fact that "very high accuracy, while desirable, is not essential since most design changes are incremental variations from a baseline". Therefore, since our research is not directly focused on the ventilation performance of the building block, but on the methodology to optimise the parameters that will improve the built environment, a constant inlet velocity profile may be accepted.

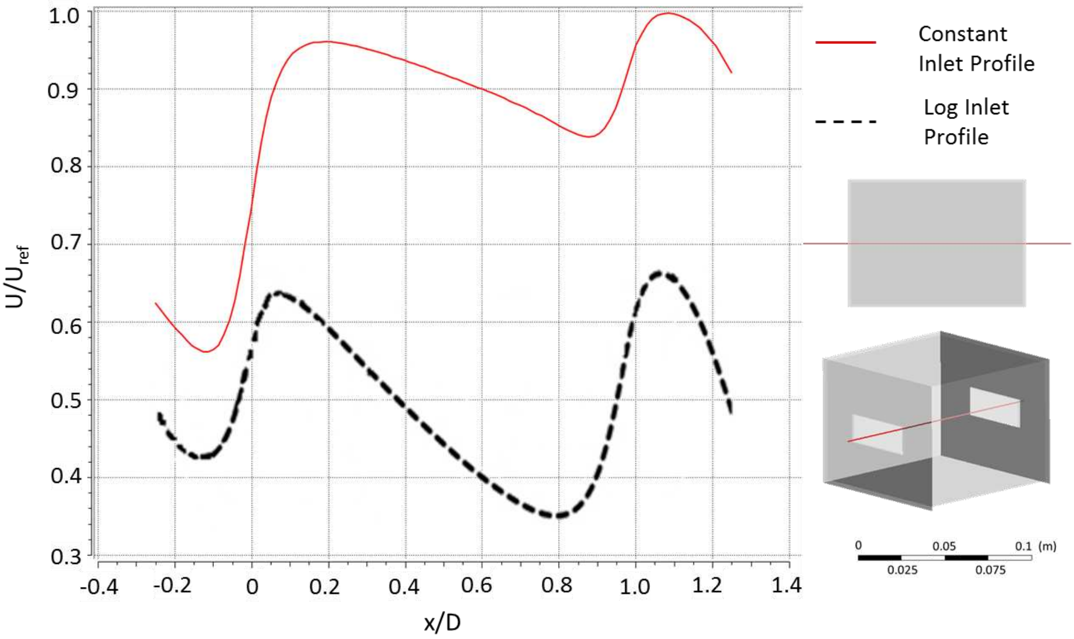

Figure 6 Velocity profile at a longitudinal line in the middle of the building block.

4.7.2 Wind tunnel validation

For the validation of the numerical simulation, the wind tunnel facility of the Civil Engineering Department at the University of Leeds was used. The closed-loop wind tunnel is 5.6 m long, with test section dimensions of 0.5m x 1.0m x 0.5m (W x L x H) [39]. The performance assessment of the model was based on velocity measurements on specific locations inside the building block and outside the window openings, as illustrated in Figure 7.

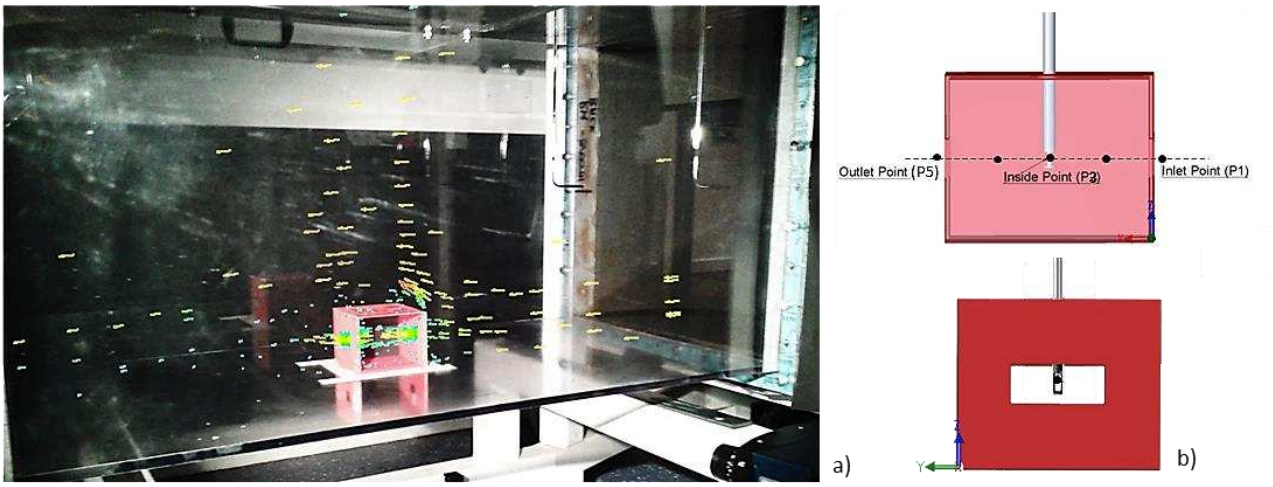

Figure 7 Model positioning in the wind tunnel test section and CFD velocity vectors indicating airflow distribution (a); hot wire measurement points of velocity speeds (b).

A uniform velocity profile of 3 m/s was achieved, identical to the one used for the numerical simulation. The speed measurements were conducted using a hot wire probe (Testo 425), obtaining results with ±1.0% rdg accuracy at velocity values of ≤ 8m/s. For each measurement point, five repeated measurements of 2 min duration were performed to reduce the human error factor. The hot wire was placed on the exact proximity of the windward and leeward window openings and in three symmetric internal positions of the building model. The results obtained are presented in Table 4 and Figure 8.

Table 4. Comparison of velocity magnitudes in five building locations from wind tunnel measurements and CFD simulation.

Measurement Point	**P1 (-0.03m)** 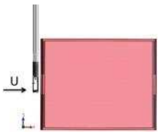	**P2(0.024m)** 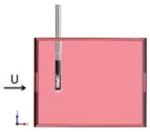	**P3 (0.05m)** 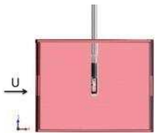	**P4(0.074m)** 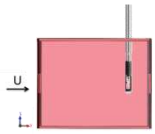	**P5 (0.013m)** 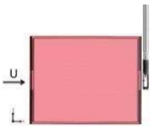
W.T. Velocity	1.95 m/s	2.66 m/s	2.67 m/s	2.36 m/s	2.54 m/s
CFD Velocity	1.84 m/s	2.87 m/s	2.76 m/s	2.59 m/s	2.97 m/s
Error	5.9 %	7.3 %	3.3 %	8.9 %	14.5 %

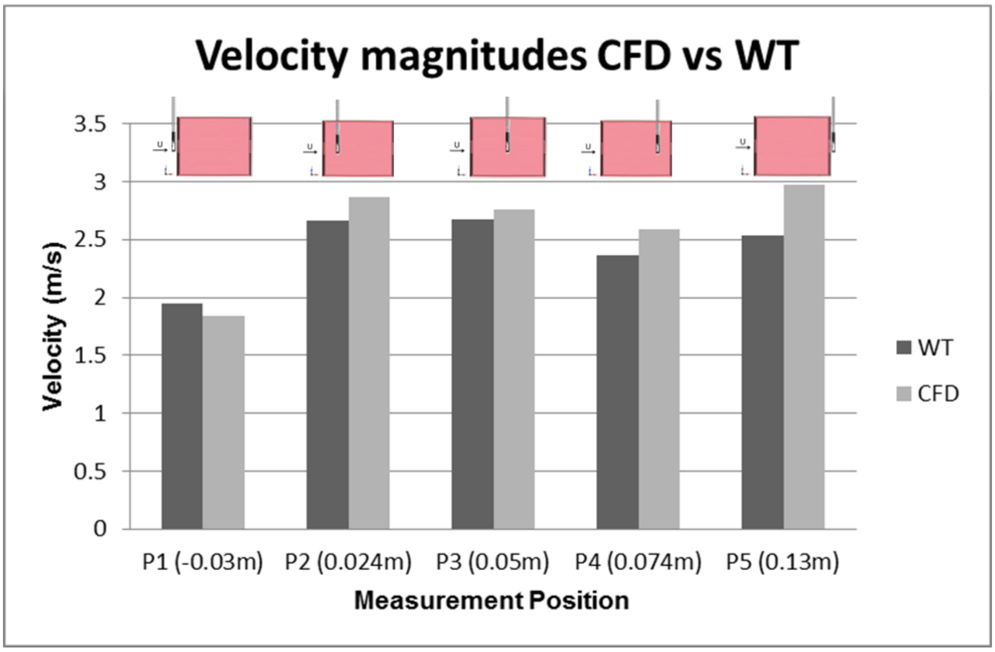

Figure 8 Graphical comparison of velocity magnitudes obtained by CFD and WT experiments in five measurement points.

According to the velocity values obtained from the wind tunnel experiments, the k-ε model performs well, validating the CFD methodology followed for the wind flow simulation. The generated errors of 5.9% and 3.3%, at the inlet and the interior of the building, are within acceptable limits, if we take under consideration the human, experimental and mechanical errors. The highest recorded error of 14.5% at the outlet (P5) can be explained by the induced turbulence in the leeward underpressure region of the building block that increases the uncertainty of both numerical and experimental value.

5. RSM metamodel methodology

The Response Surface Optimisation technique is a simulation driven optimisation tool that enables the exploration of various design parameters and displays the interactions among them and the resulting solutions. A DoE study was performed and combined with RSM, in ANSYS Design Exploration 15.0. The methodology followed for the identification of the optimum design solution can be summarised in steps 1 to 4, as shown in Table 5, and has doable extension to similar design exploration problems.

Table 5. Workflow for optimization methodology

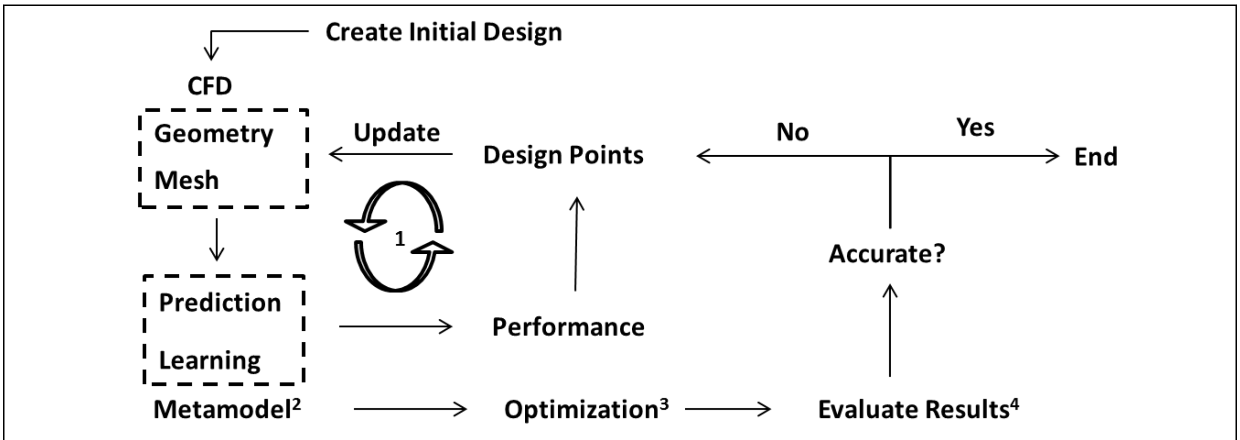

Step 1.	Design of Experiments
i.	Define Input Parameters: continuous or discrete
ii.	Define Output Parameters
iii.	Select DoE Scheme: Central Composite Design, Box-Behnken Design, etc.
iv.	Select Design Type: Auto Defined, Face-Centered, etc.
v.	Generate Design Points
Step 2.	Response Surface
vi.	Select a Meta Model: Standard Response Surface, Kriging, Neutral Network etc.
vii.	Generate Correlation of Parameters, Sensitivity Results, etc.
Step 3.	Optimization
viii.	Select Optimization Method: Screening, MOGA or NLPQL.
ix.	Define Objectives and Constrains
x.	Obtain Candidate Points
Step 4.	Robustness Evaluation
xi.	Perform Six Sigma Analysis (SSA)

5.1 RSM set up

Once the input building design is created and the primary simulation run is completed (as presented in section 4), the optimization problem can be modelled. The first step concerns the identification of the input independent variables, their design space (or constraints), as well as the output dependent variables (Table 6). In the case of cross-ventilated buildings, the window positioning and window configuration has been found to play a determinant role in enhancing natural ventilation efficiency (Stavrakakis et al., 2012; Bangalee et al., 2013). Therefore, in consideration of the predicted results, the dimensional characteristics of the window openings, the width and height, were selected as the input continuous parameters. Additional derived input parameters were defined in order to keep the windows always centralised regardless configuration. The design space, within which the exploration of several design alternatives would be performed, was defined based on rational criteria. The range of the input variables was from 0.01 m to 0.018 m for the window height and from 0.023 m to 0.046 m for the window width. Output parameters were set the flow rate through the front window opening and the homogeneity of the flow inside the room, represented by the standard deviation of velocities.

Table 6. Quantification of input and output parameters

Parameters		**Name**	**Initial Value**	**Constrains**
Input	**P1**	Window_Height	0.018 m	0.01 m≤ **P1** ≤0.018 m
	P2	Window_Width	0.046 m	0.023 m≤ **P2** ≤0.046 m
	P3	Horizontal_Dist	0.027 m	**P3** =(0.1-**P2**)/2
	P4	Vertical_Dist	0.031 m	**P4** =(0.08-**P1**)/2
Output	**P5**	Flow_Rate_Q	1.81 x10^{-3} m^3/s	
	P6	St_Dev_Sensor_Vel	0.512 m/s	

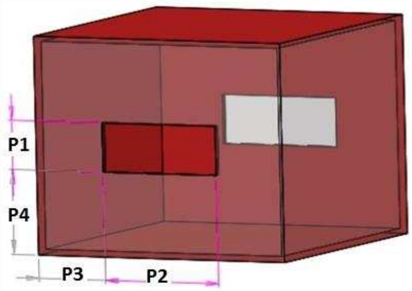

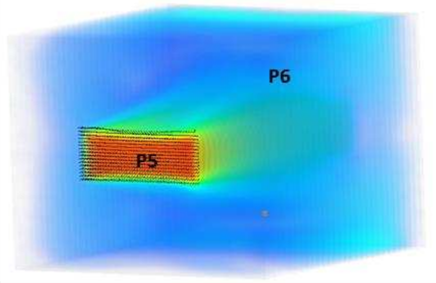

Graphical representation of input (left) and output (right) parameters

After having defined the number of input and output parameters, the generation of the design points was performed using the Auto-defined Central Composite Design (CCD) scheme. The CCD consists of one central point, 2N star (or axial) points and a two-level full factorial design (2^N factorial points) [18]. The number of the design points can be determined by Eq. (10)

$$DP = 1 + 2N + 2^N \qquad \text{Eq. (10)}$$

where N is the number of input parameters (or factors).

The selected scheme enabled the creation of 9 rotatable and symmetrical designs, including the initial one. The calculation of their responses was the most time consuming part of the study, as they were solved sequentially to achieve convergence in every simulation run. The results obtained are listed in Table 7 and represent the design space within which the quadratic response surface was constructed.

Table 7. CCD-based Design Points and their obtained CFD solutions

Design Point	**P1 (m) Window_Height**	**P2 (m) Window_Width**	**P5 (m^3/s) Flow_Rate_Q**	**P6 (m/s) St_Dev_Sensor_Vel**
1 (DP 6)	0.014	0.0345	1.01 $\times 10^{-3}$	0.443
2 (DP 2)	0.01	0.0345	0.69 $\times 10^{-3}$	0.380
3 (DP 8)	0.018	0.0345	1.34 $\times 10^{-3}$	0.491
4 (DP 4)	0.014	0.023	0.66 $\times 10^{-3}$	0.438
5 (DP 5)	0.014	0.046	1.37 $\times 10^{-3}$	0.469
6 (DP 1)	0.01	0.023	0.46 $\times 10^{-3}$	0.374
7 (DP 7)	0.018	0.023	0.87 $\times 10^{-3}$	0.477
8 (DP 3)	0.01	0.046	0.93 $\times 10^{-3}$	0.402
9 (DP 0)	0.018	0.046	1.81 $\times 10^{-3}$	0.512

The second step was the selection of a Response Surface Type algorithm. For the purpose of this, the Standard Response Surface was adopted, allowing the implementation of a regression analysis to generate a second-order fitted response for estimating the correlations among the selected parameters. The second-order models are commonly used for optimisation processes, due to their flexible nature and ability to perform better in complex problems (Myers et al., 2009). In this stage, the relationships between the independent and dependent parameters can be investigated, by providing a graphical insight into the design sensitivity analysis.

Next to the optimization problem was the selection of the objective function and the optimisation algorithm. The objective of the optimization was to improve the natural ventilation efficiency. This could be achieved by increasing the flow rate and also by promoting the flow homogeneity in the area of interest. Thus, the resulting optimization aims were to maximise Flow_Rate_Q (P5) and simultaneously minimise St_Dev_Vel (P6), within the restricted range values set for the window height (P1) and width (P2). The Screening optimization algorithm was used, which is based on the simple concept of sampling and sorting, identifying the most significant and influential variables, regarding the predefined objectives and constraints [43]. 1,000 uniformly distributed sample sets were generated for correlation, within the optimization domain, which constitutes one of the main benefits of this method. Figure 9 illustrates the evolution of the sample sets by a red curve and the location of the design sample points in the predefined design space by a blue dot.

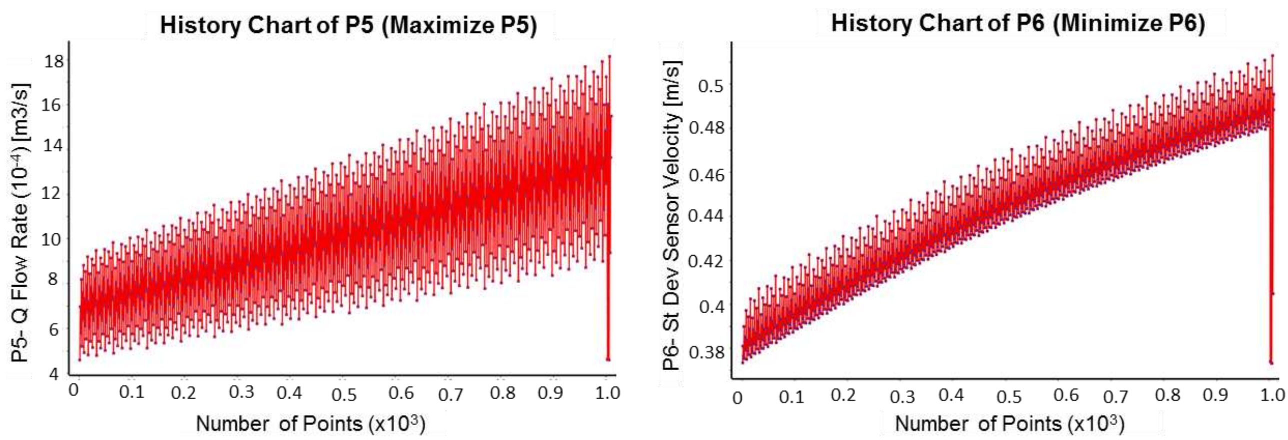

Figure 9 History chart of the sampling design points for the two output parameters; Flow Rate (left) and Standard Deviation of velocities (right).

5.2 RSM results

The generated response surface was evaluated against its quality and accuracy by the response surface's Goodness of Fit. Figure 10 (top) illustrates the fit of the regressed model on the response function, by plotting the predicted response values versus the observed values from the design points.

The Goodness of Fit also enabled the evaluation of the performance of the selected meta-modeling algorithm. The coefficient of determination (R^2) was equal to 1 (or 100%) for the flow rate and equal to 0.9989 (or 99.89%) for the standard deviation, indicating a well-represented response surface by the parametric model. However, the verification point for the flow rate showed a small deviation from the diagonal line, indicating the need to refine the response surface. After taking under consideration this point to the response surface, the updated Goodness of Fit (Figure 10 bottom) resulted to an improved response surface with a reduction of the maximum relative residuals from 13.77% to 0.21% for the flow rate and from 0.42% to 0.19% for the standard deviation.

The RSM analysis produced estimations of the correlation between the independent and dependent parameters, based on the input and output values of the Design Points, allowing the graphical exploration of any design alternative within the constraint limits (Table 8 a). It also permitted the quantification of the relationship between the input variables and their responses (Table 8 b, c). The predicted coefficients of determination for every input variable indicated their impact effect on the design responses and thus gave a first insight on the sensitivity of the design solution. Furthermore, the results permitted the exploration of any design point within the design region, considering that they were values obtained from the response surface and not from actual simulation runs.

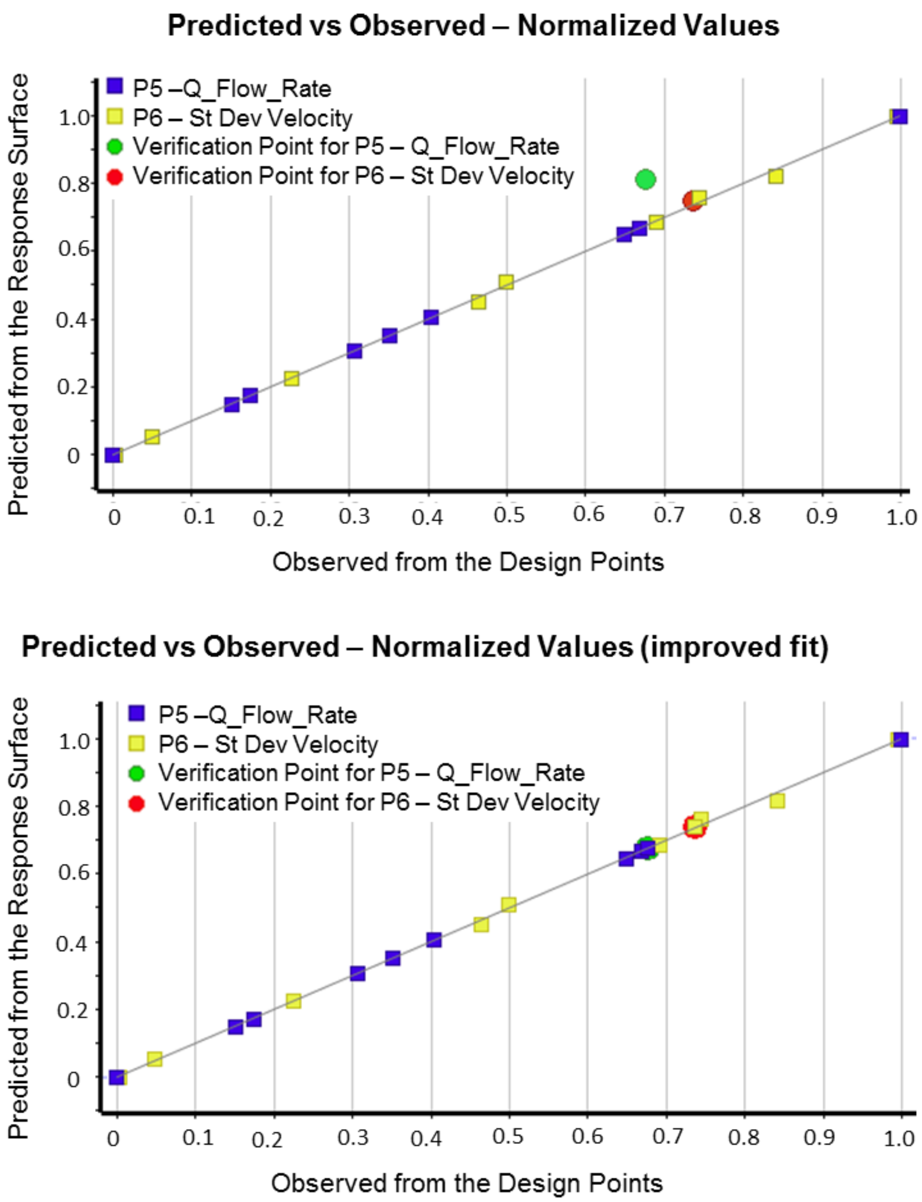

Figure 10 Goodness of fit for the estimated response surface function; initial prediction (top) and improved prediction (bottom).

Table 8. Results of Standard Response Surface algorithm

a) Response Chart – Graphical response exploration of any design alternative within the constraint limits

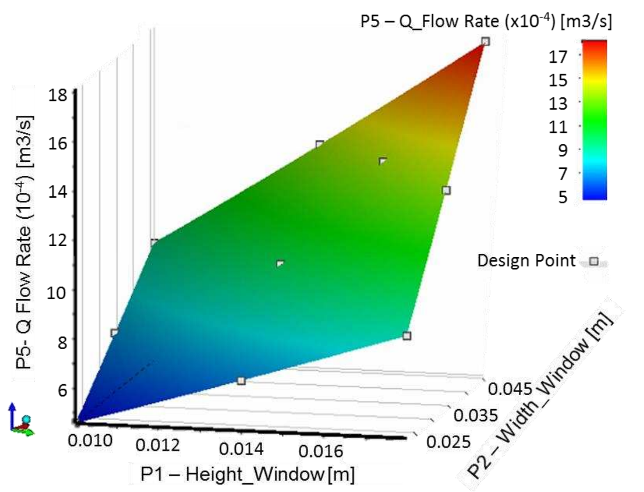

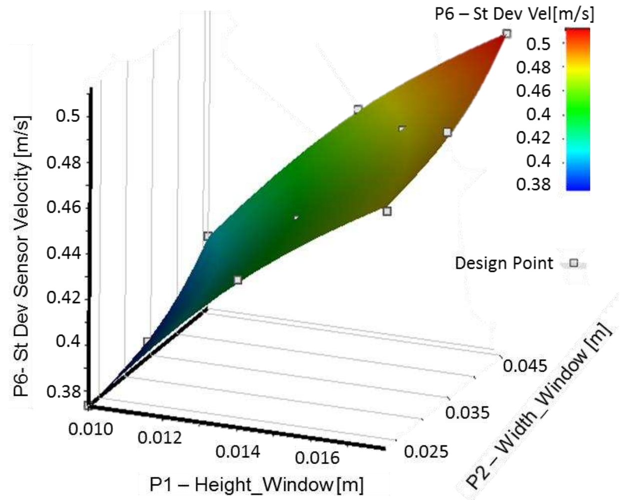

b) Local Sensitivity Chart – Impact chart of input on output parameters

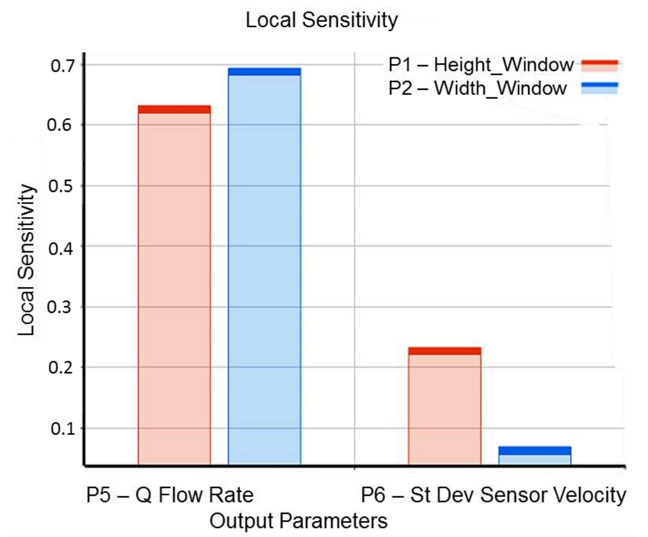

c) Spider Chart – Impact of variable input parameters on all output parameters

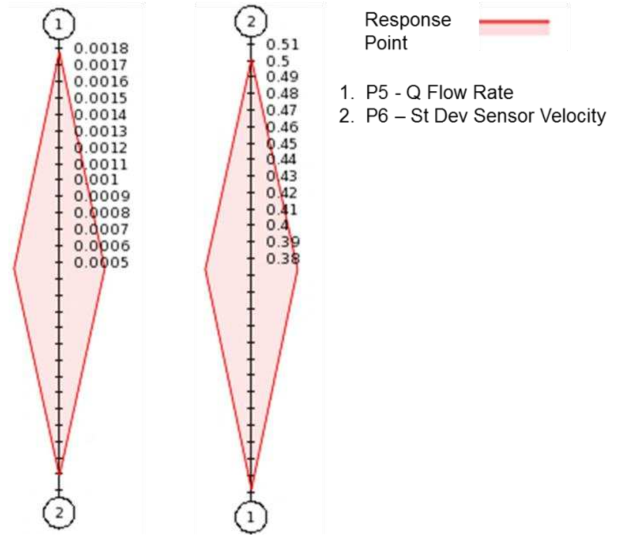

d) Local Sensitivity Curves – Variation of design points response, based on the Local Sensitivity Chart

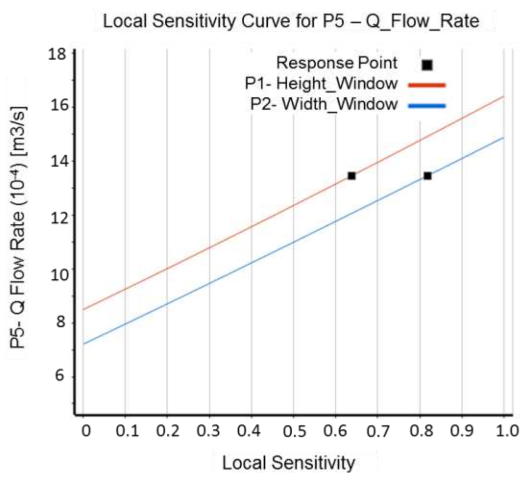

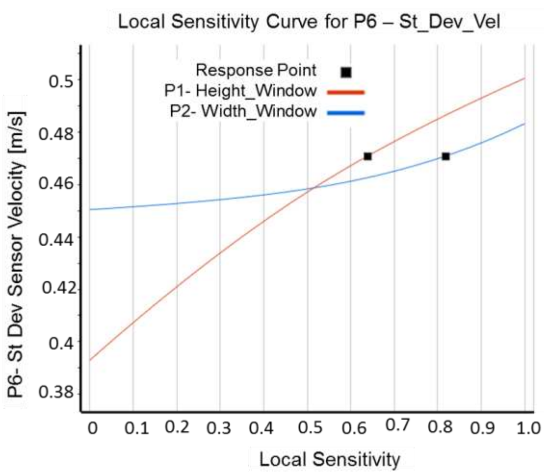

5.3 Correlation of parameters

A Parameters Correlation analysis was conducted, in order to assess the impact role of each input parameters on the design outputs and ascribe the degree of quadratic correlation between two parameters, with either a linear or quadratic trend, using the Spearman's rank correlation[2]. The implementation required the generation of 60 unique and randomly selected design sets, based on Latin Hypercube Sampling (LHS) method, according to which the input parameters have at least 5% deviation of correlations.

As indicated in Table 9, the window height emerges to be the most influential parameter when the standard deviation is evaluated, with correlation value of 96.9%, compared to 12.35% for the window width. While in the flow rate, the window width prevails slightly over the window height with correlation values equal to 73.6% and 55.7%, respectively.

Table 9. Linear correlation matrix and estimated correlation values between parameters

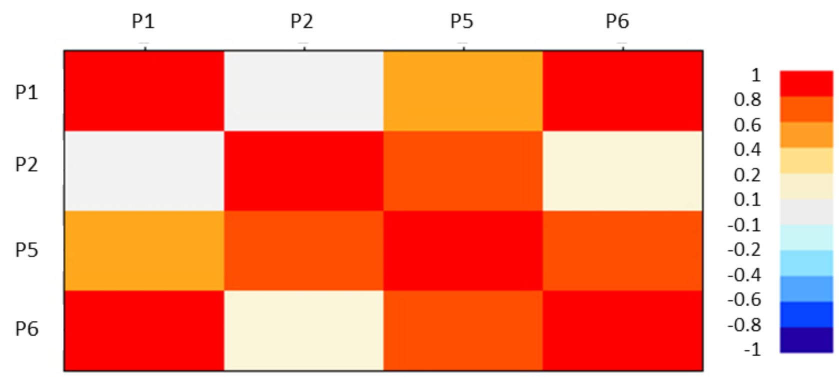

Correlation	Value
P1 – P5	55.68 %
P2 – P5	73.62 %
P1 – P6	96.94 %
P2 – P6	12.35 %

P1 = Window_Height
P2 = Window_Width
P5 = Flow_Rate (Q)
P6 = St_Dev_Sensor_Vel (SD)

Scatter plots were also produced to identify the degree to which the regression lines represent the model data. Figure 11 illustrates the generated linear and quadratic trend lines for each parameter pair. The multiple regression analysis showed that quadratic trend lines were a better fit for the input variables. The estimated coefficients of determination (R^2) showed that 39.9% and 54.6% of the Flow_Rate variation can be explained by the variation of the Window_Height and Window_Width, respectively. The variability of the Standard_Deviation can be strongly explained by the

[2]Spearman's rank correlation is used to identify the relationship between parameters that belong in complex nonlinear data sets, without taking under consideration the outliers [44].

Window_Height with a percentage of 92.1%, as opposed to the Window_Width that gave a poor coefficient of determination equal to 12.9%.

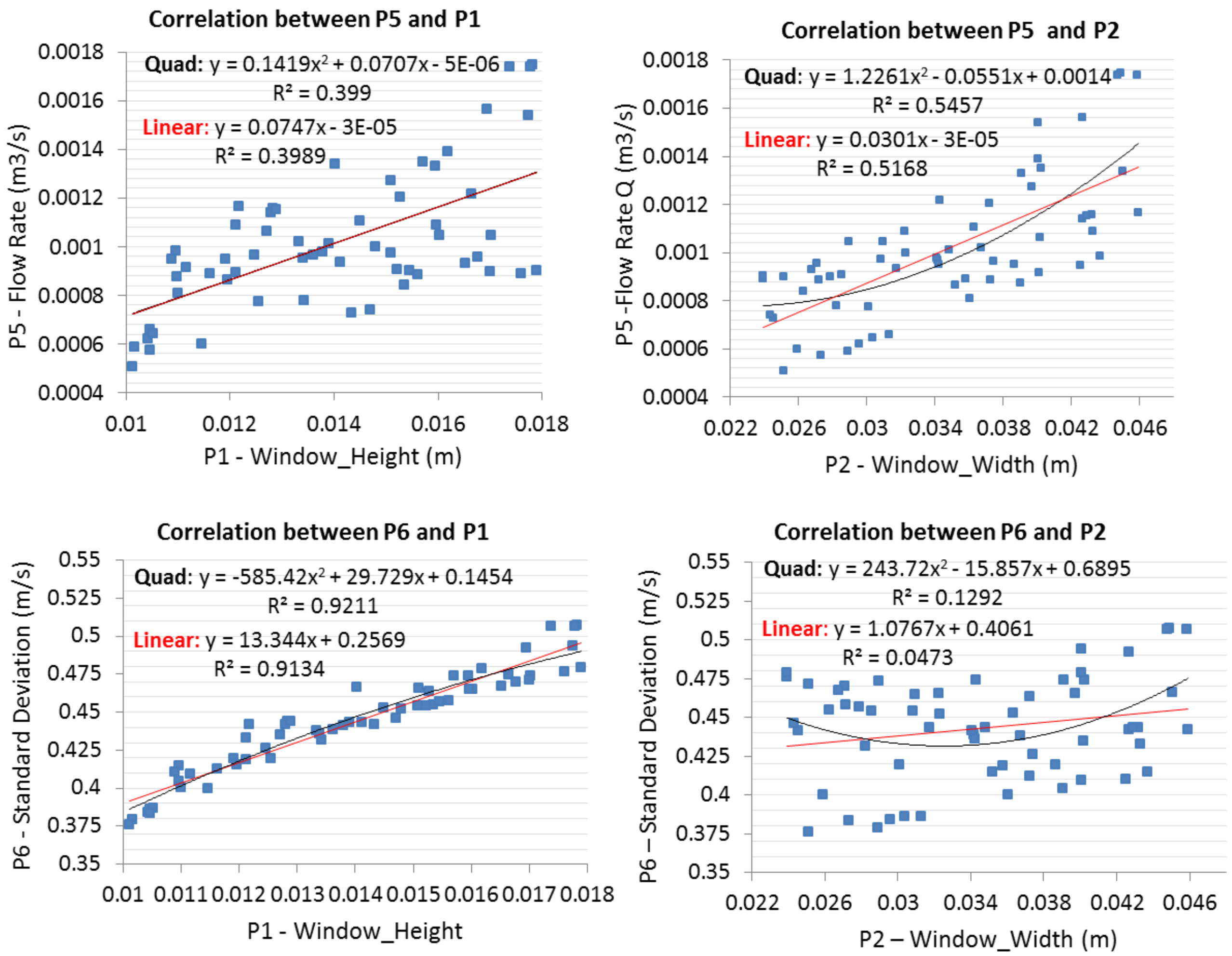

Figure 11 Correlation charts with quadratic and linear trend lines for the Flow Rate (top) and the Standard Deviation of Velocities (bottom)

5.4 Optimization results

On the improvement of the ventilation performance, the Screening optimisation method was employed that allowed the generation of 1,000 window design samples to be evaluated against the objective set. The optimisation results contained information about the candidate optimum design solutions, Pareto optimality and sensitivities analysis of the studied parameters. Figure 12 illustrates the generated design space, where feasible design solutions exist. Tradeoff charts, also known as Pareto fronts, enable the exploration of the best (blue), worst (red), feasible and infeasible designs.

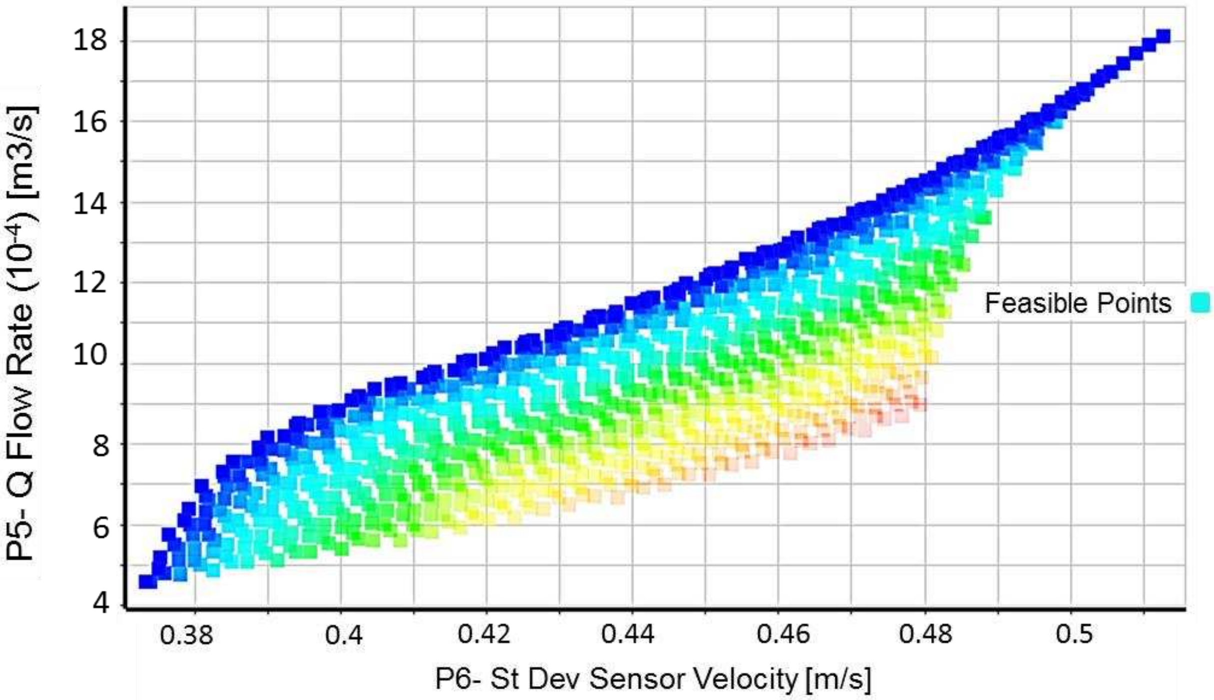

Figure 12 Two-dimensional Tradeoff chart displaying feasible design points.

Table 10 shows the three generated candidate design points that show the best behaviour regarding the predefined set of objectives and constraints. According to the results, all three candidate points produced similar results for the standard deviation, with maximum variation of 3.64% between CP1 and CP3. On the other hand, the flow rate varied over 12.67% between these two points, which makes the CP3 to satisfy most the established objectives for maximizing the flow rate and minimizing the standard deviation.

Table 10. Candidate Points generated from the Screening method

Candidate Points	**P1 (m) Window_Height**	**P2 (m) Window_Width**	**P5 (m^3/s) Flow_Rate_Q**	**P6 (m/s) St_Dev_Vel**
Candidate Point 1	10.03×10^{-3}	40.26×10^{-3}	0.818×10^{-3}	0.390
Candidate Point 2	10.06×10^{-3}	43.14×10^{-3}	0.882×10^{-3}	0.397
Candidate Point 3	10.00×10^{-3}	46.00×10^{-3}	0.937×10^{-3}	0.405

The dimensions of the optimum window opening are 0.01m height and 0.046m width. The values of the output parameters over the initial design deviate -48% and -21% for the flow rate and the standard deviation respectively. It is worth highlighting that the flow rate was not maximized, but minimized in order to achieve local optimality.

5.5 Robust Analysis

On the impact identification of the uncontrollable parameters on the design response, a robust design analysis was performed. The robust design consists of a Six Sigma Analysis that investigates the performance of the predicted response surface, by incorporating factors, uncertainties and assumptions that are not taken under consideration during the RSM analysis. Thus, the robustness of the model presupposes an unattained design, regarding the possible biases due to model misspecification and misstatements and the distribution of the error [45].

The Six Sigma Analysis followed the same steps and settings used in the Design of Experiments and the Response Surface (refer to Table 5); with the main difference being that the inputs variables were treated as uncertainty parameters. The LHS method was adopted for the generation of 100 samples and the obtained results were focused on the sensitivities of output variables with respect to the input parameters and the statistical distribution of the samples responses.

The sensitivity graph produced was not representative of the local sensitivities (such as in Table 9), but of the global statistical sensitivities, irrespective of the values of input parameters. As illustrated in Table 11, the sensitivity correlation coefficients highlighted the window width to affect most the flow rate with a value of 75.57% and the window height to maintain the highest impact role on the Standard Deviation response, with a correlation coefficient equal to 82.06%. It is worth mentioning that when the factor of the Standard Deviation was assessed, the window width appears to have an increased strength of correlation (54.04%) when compared with the one obtained from the RS analysis (12.35%) (see Table 9).

Table 11. SSA statistical sensitivities for the output parameters

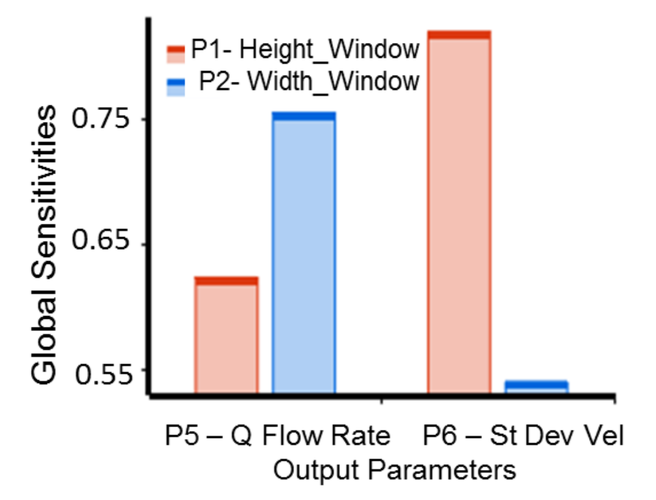

Correlation	R^2
P1 – P5	62.39%
P2 – P5	75.57%
P1 – P6	82.06%
P2 – P6	54.04%

P1 = Window_Height
P2 = Window_Width
P5 = Flow_Rate (Q)
P6 = St_Dev_Vel (SD)

In order to prove the robustness of the model, the Six Sigma quality criterion needs to be satisfied. According to this, the output parameters should lie within the lower and upper specification limits of a Gaussian distribution. According to Figure 13, in the flow rate distribution the highest probability density is in the range of 0.97×10^{-3} m^3/s. The distribution is positively skewed and slightly flat, with a skewness value of 0.22 and a kurtosis value of -0.55, approximating the graph of the normal distribution. The standard deviation distribution shows a negative skewness of -0.23 and a small kurtosis of -0.007, with the maximum probability density to lie in the range of the mean value (0.44 m/s) that gives the image of normal distribution.

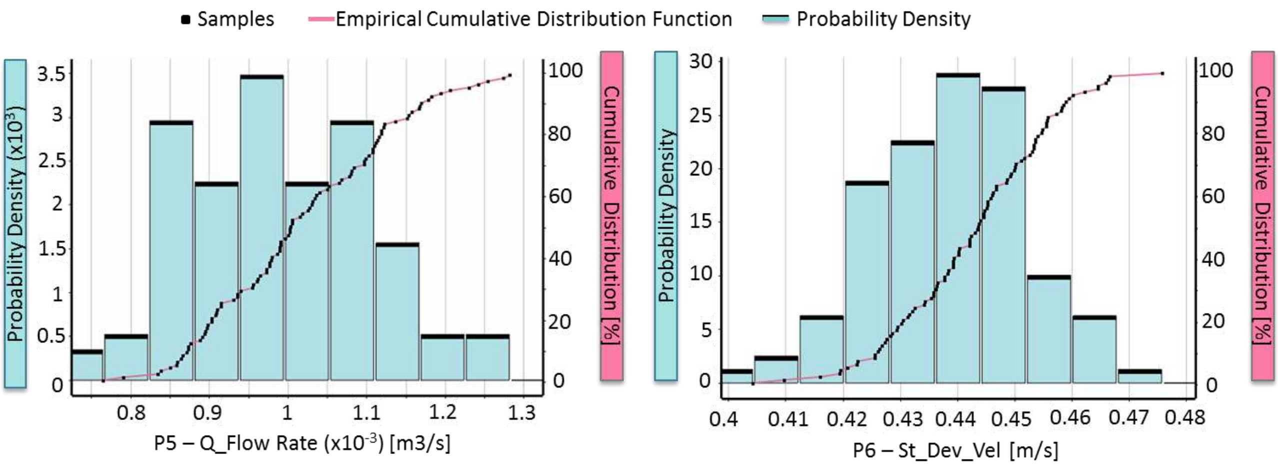

Figure 13 Statistical distribution functions for P5_Flow_Rate (left) and P6_St_Dev_Vel (right).

5.6 RSM optimization verification

The verification of the optimization method concerns the comparison of the values estimated for the output parameters by the RSM metamodel and those obtained by the CFD simulation runs for the three candidate points. The calculated design solutions from the numerical simulation are presented in Table 12.

Table 12. Verification of the optimization-generated Candidate Points

Candidate Points	**Candidate Point 1 RSM | CFD**		**Candidate Point 2 RSM | CFD**		**Candidate Point 3 RSM | CFD**	
Window Height (m)	10.03×10^{-3}		10.06×10^{-3}		10.00×10^{-3}	
Window Width (m)	40.26×10^{-3}		43.14×10^{-3}		46.00×10^{-3}	
Flow_Rate ($\times 10^{-3}$ m^3/s)	0.818	0.837	0.882	0.901	0.937	0.9362
St_Dev_Vel (m/s)	0.390	0.406	0.397	0.414	0.4047	0.4049

According to the results, the values of both flow rate and standard deviation for the CP1 and CP2 were underestimated over a maximum of 4.8%. The CP3 seems to be the optimum one for our case study, since it maintains the lowest value of standard deviation and the highest flow rate, satisfying the set of optimisation objectives.

The verification of the results enabled the production of two different error indicators. As shown in Table 13, the maximum error for the flow rate was equal to 4.28% and the one for the standard deviation equal to 2.32%, proving the high quality optimization results, verifying at the same time the Response Surface Methodology study.

Table 13. Error between CFD and RSM results for the three candidate points

Candidate Point	**Error Flow_Rate**	**Error St_Dev_Vel**
Candidate Point 1	2.32 %	4.10 %
Candidate Point 2	2.15 %	4.28 %
Candidate Point 3	0.03 %	0.07 %

6. Discussion

The RSM metamodel-based optimization technique allows the determination of the response of several design variables after approximating a response function, averting the need for time-consuming parametric studies [46]. It is a valuable tool when the relationship of the independent variables needs to be assessed, regarding multiple design responses. However, the RSM method should be carried out with extreme caution, when targets to the identification of those conditions that will achieve the maxima or minima of the response function.

The arbitrary selection of the independent (input) variables is pre-dominantly user-based, and the optimization of one response criterion does not always presuppose the optimization of other criteria of the model and vice versa. Also the number of the selected parameters is of great importance, since it determines the number of the studied design points, upon which the response surface function will be based. Thus, the type and the number of the input parameters should always be selected after rational consideration, in order to maximise the quality of the results within reasonable computational time.

Moreover, the conduction of the DoE study, within a certain design space, bounded by dimensional constraints, can only conclude to improved design solutions, or local optimal, which sometimes may abstain from the global optimal solution.

The current investigation conducted a RSM metamodel-based optimization technique, using the ANSYS commercial platform. The main aim was the presentation of a validated analysis of experiments for the identification of improved (or locally optimal) conditions in the building's interior environment, based on a set of controllable variables. For this purpose, a CCD design was adopted for fitting a second order response surface regression model. The problem set was a two response optimization, including the maximization of the flow rate from the frontal window opening and the minimization of the standard deviation of internal velocities, deeming to a homogeneous ventilation rate inside the building block.

In the first step a CFD simulation study on the wind distribution inside and outside the building block was performed, followed by wind tunnel velocity measurements that validated the methodology and the k-ε turbulence model used.

In the DoE study, nine design points were generated and the produced response function revealed the estimated relationships and correlations of input and output parameters. The flow rate was more influenced by the window width, rather than the window height with correlation coefficients of 73.62% and 55.68% respectively, as compared to the standard deviation, for which the window height was the predominant factor of the response with a correlation coefficient of 96.94%, as opposed to 12.35% for the window width.

The robust assessment, performed by the Six Sigma Analysis, revealed a reliable curve-fitted model and arising extrapolation errors due to unrepresentative samples' selection or sampling error were small to make the analysis imprecise.

Finally, the multi-objective optimization highlighted three candidate points with the most favourable behaviour for the improvement of indoor airflow conditions. Their verification was valuable, because even if the deviation of the results was small, it was important to prove the accuracy of the methodology.

7. Conclusion

The verified solution of the optimal design for the window opening indicated that improved indoor airflow condition inside the building block, as described by the ventilation rate and the airflow homogeneity, was obtained by a 0.046 m wide and 0.01 m height opening characteristics. It was also concluded that both dimensional parameters were influencing the design solution on a different level. Coupled CFD and optimizations techniques were found to be important tools for the analysis and evaluation of multiple parameters and responses, producing comparative results that may assist decision-making process towards improved (if not optimum) design solutions. Finally, it was deduced that the presented methodology can be successfully used in studies of the built environment, allowing users to select throughout a plethora of parameters that are relevant to the equivalent case study.

8. References

[1]. N. P. Suh, The Principles of Design, vol. 226. Oxford University Press, 1990, p. 401.

[2]. X. Shen, G. Zhang, and B. Bjerg, “Investigation of response surface methodology for modelling ventilation rate of a naturally ventilated building,” Building and Environment, vol. 54, pp. 174–185, 2012.

[3]. M. Hajdukiewicz, M. Geron, and M. M. Keane, “Calibrated CFD simulation to evaluate thermal comfort in a highly-glazed naturally ventilated room,” Building and Environment, vol. 70, pp. 73–89, 2013.

[4]. S. Wang and D. Zhu, “Application of CFD in retrofitting air-conditioning systems in industrial buildings,” Energy and Buildings, vol. 35, no. 9, pp. 893–902, 2003.

[5]. J. K. Calautit and B. R. Hughes, “Wind tunnel and CFD study of the natural ventilation performance of a commercial multi-directional wind tower,” Building and Environment, vol. 80, pp. 71–83, 2014.

[6]. T. Zhang, H. Zhou, and S. Wang, “An adjustment to the standard temperature wall function for CFD modeling of indoor convective heat transfer,” Building and Environment, vol. 68, pp. 159–169, 2013.

[7]. J. Srebric, V. Vukovic, G. He, and X. Yang, “CFD boundary conditions for contaminant dispersion, heat transfer and airflow simulations around human occupants in indoor environments,” Building and Environment, vol. 43, no. 3, pp. 294–303, 2008.

[8]. S. Murakami, R. Ooka, A. Mochida, S. Yoshida, and Sangjin Kim, “CFD analysis of wind climate from human scale to urban scale,” Journal of Wind Engineering and Industrial Aerodynamics, vol. 81, no. 1–3. pp. 57–81, 1999.

[9]. S. Kato, S. Murakami, A. Mochida, S. Akabayashi, and Y. Tominaga, “Velocity-pressure field of cross ventilation with open windows analyzed by wind tunnel and numerical simulation,” Journal of Wind Engineering and Industrial Aerodynamics, vol. 44, no. 1–3. pp. 2575–2586, 1992.

[10]. C. R. Chu and B. F. Chiang, “Wind-driven cross ventilation in long buildings,” Building and Environment, vol. 80, pp. 150–158, 2014.

[11]. B. Blocken, “50 years of Computational Wind Engineering: Past, present and future,” Journal of Wind Engineering and Industrial Aerodynamics, vol. 129, pp. 69–102, 2014.

[12]. G. M. Stavrakakis, P. L. Zervas, H. Sarimveis, and N. C. Markatos, “Optimization of window-openings design for thermal comfort in naturally ventilated buildings,” Applied Mathematical Modelling, vol. 36, no. 1, pp. 193–211, 2012.

[13]. X. Shen, G. Zhang, and B. Bjerg, “Assessments of experimental designs in response surface modelling process: Estimating ventilation rate in naturally ventilated livestock buildings,” Energy and Buildings, vol. 62, pp. 570–580, 2013.

[14]. T. Norton, J. Grant, R. Fallon, and D. W. Sun, “Optimising the ventilation configuration of naturally ventilated livestock buildings for improved indoor environmental homogeneity,” Building and Environment, vol. 45, no. 4, pp. 983–995, 2010.

[15]. T. W. Simpson, J. D. Poplinski, P. N. Koch, and J. K. Allen, “Metamodels for Computer-based Engineering Design: Survey and recommendations,” Engineering With Computers, vol. 17, no. 2. pp. 129–150, 2001.

[16]. H. Hotelling, “Experimental Determination of the Maximum of a Function,” The Annals of Mathematical Statistics, vol. 12, no. 1, pp. 20–45, 1941.

[17]. M. Friedman; and L. J. Savage, “Planning Experiments Seeking Maxima,” in Techniques of Statistical Analysis, M. H. and W. A. C. Eisenhart and Wallis, Eds. N.York-London: McGraw-Hill, 1947, pp. 363–72.

[18]. W. C. R. Myers, A. Khuri, “Response Methodology :,” Technometrics, vol. 31, no. 2, pp. 137–157, 1988.

[19]. G. E. P. Box and K. B. Wilson, “On the Experimental Attainment of Optimum Conditions,” Journal of the Royal Statistical Society, vol. 13, no. 1, pp. 1–45, 1951.

[20]. R. Fegade and V. Patel, “Unbalanced Response and Design Optimization of Rotor by ANSYS and Design of Experiments,” International Journal of Scientific & Engineering Research, vol. 4, no. 7, pp. 1521–1535, 2013.

[21]. J. Plackett, R., Burman, “The Design of Optimum Multifactorial Experiments,” Biometrika, vol. 33, no. 4, pp. 305–325, 1946.

[22]. P. Mandloi and G. Verma, “Design Optimization of an in-Cylinder Engine Intake Port,” in Nafems World Congress 2009, 2009.

[23]. K. C. Ng, K. Kadirgama, and E. Y. K. Ng, “Response surface models for CFD predictions of air diffusion performance index in a displacement ventilated office,” Energy and Buildings, vol. 40, pp. 774–781, 2008.

[24]. P. Karava, T. Stathopoulos, and A. Athienitis, “Airflow assessment in cross-ventilated buildings with operable façade elements”. Building and Environment, vol. 46, no 1, pp.266-279, 2011.

[25]. S. Driss, Z. Driss and I. Kallel Kammoun, 'Numerical simulation and wind tunnel experiments on wind-induced natural ventilation in isolated building with patio', Energy, vol. 90, pp. 917-925, 2015.

[26]. N. Wong and S. Heryanto, 'The study of active stack effect to enhance natural ventilation using wind tunnel and computational fluid dynamics (CFD) simulations', Energy and Buildings, vol. 36, no. 7, pp. 668-678, 2004.

[27]. M. Mora-Pérez, I. Guillén-Guillamón and P. López-Jiménez, 'Computational analysis of wind interactions for comparing different buildings sites in terms of natural ventilation', Advances in Engineering Software, vol. 88, pp. 73-82, 2015.

[28]. J. Song and X. Meng, 'The Improvement of Ventilation Design in School Buildings Using CFD Simulation', Procedia Engineering, vol. 121, pp. 1475-1481, 2015.

[29]. G. Carrilho da Graça, Q. Chen, L. R. Glicksman, and L. K. Norford, "Simulation of wind-driven ventilative cooling systems for an apartment building in Beijing and Shanghai," Energy and Buildings, vol. 34, no. 1, pp. 1–11, 2002.

[30]. S. Driss, Z. Driss and I. Kallel Kammoun, 'Impact of Shape of Obstacle Roof on the Turbulent Flow in a Wind Tunnel', American Journal of Energy Research, vol. 2, no. 4, pp. 90-98, 2014.

[31]. L. James Lo, D. Banks and A. Novoselac, 'Combined wind tunnel and CFD analysis for indoor airflow prediction of wind-driven cross ventilation', Building and Environment, vol. 60, pp. 12-23, 2013.

[32]. J. Calautit, and B. Hughes, "Measurement and prediction of the indoor airflow in a room ventilated with a commercial wind tower," Energy and Buildings, vol 84, pp.367-377, 2014.

[33]. J. Calautit, and B. Hughes, "Wind tunnel and CFD study of the natural ventilation performance of a commercial multi-directional wind tower", Building and Environment, 80, pp.71-83, 2014.

[34]. Z. Q. Thai, W. Zhang, Z. Zhang, and Q. Y. Chen, "Evaluation of various turbulence models in predicting airflow and turbulence in enclosed environments by CFD: part 1 -

Summary of prevalent turbulence models," HVAC & R Research, vol. 13, no. 6, pp. 853–870, 2007.

[35]. D. O'Connor, J. Calautit, and B. Hughes, "A study of passive ventilation integrated with heat recovery", Energy and Buildings, 82, pp.799-811, 2014.

[36]. R. Ramponi and B. Blocken, 'CFD simulation of cross-ventilation for a generic isolated building: Impact of computational parameters', Building and Environment, vol. 53, pp. 34-48, 2012.

[37]. Q. Chen and J. Srebric, 'A Procedure for Verification, Validation, and Reporting of Indoor Environment CFD Analyses', HVAC&R Res., vol. 8, no. 2, pp. 201-216, 2002.

[38]. R. I. Bates, P. D., Lane, S. N. and Ferguson, Computational fluid dynamics. Chichester, UK: John Wiley & Sons, Ltd, 2005.

[39]. J. K. Calautit, H. N. Chaudhry, B. R. Hughes, and L. F. Sim, "A validated design methodology for a closed-loop subsonic wind tunnel," Journal of Wind Engineering and Industrial Aerodynamics, vol. 125, pp. 180–194, 2014.

[40]. F. Joerg, "Recommendations of the COST action C14 on the use of CFD in predicting pedestrian wind environment," Fourth International Symposium on Computational Wind Engineering, pp. 529–532, 2006.

[41]. Bangalee, M., Miau, J., Lin, S. and Yang, J. "Flow visualization, PIV measurement and CFD calculation for fluid-driven natural cross-ventilation in a scale model". Energy and Buildings, vol 66, pp.306-314, 2013.

[42]. Myers, R., Montgomery, D. and Anderson-Cook, C. (2009). Response surface methodology. Hoboken, N.J.: Wiley.

[43]. ANSYS, "Design Exploration, Release 12.1," no. November. ANSYS, Inc, Southpointe 275 Technology Drive Canonsburg, PA 15317, 2009.

[44]. Borradaile, G. (2003). Statistics of earth science data. Berlin: Springer.

[45]. A. I. Khuri and S. Mukhopadhyay, "Response surface methodology," WIREs Computational Statistics, vol. 2, pp. 128–149, 2010.

[46]. J. Cheng and Q. S. Li, "Application of the response surface methods to solve inverse reliability problems with implicit response functions," Computational Mechanics, vol. 43, pp. 451–459, 2009.